Proteomic Analysis and 2-Hydroxyisobutyrylation Profiling in Metabolic Syndrome Induced Restenosis

Authors

Xiangyu Liu, Liping Zhou, Wenjing Huang, Yanyan Yang, Yijun Yang, Tianwei Liu, Mingjin Guo, Tao Yu, and Yongxin Li

Correspondence

qduahvasc@163.com;
yutao0112@qdu.edu.cn;
alexander1985827@163.com

In Brief:

The proteomics and 2-hydroxyisobutyrylation PTMomics in the vascular tissues of metabolic syndrome induced in stent restenosis were detected. The modification sites related to smooth muscle cell contraction, PI3K-AKT signaling, and platelet activation were significantly reduced, while those related to HIF-1 signaling, lipid metabolism, and atherosclerosis were increased. These site differences may provide key insights for new treatment methods to alleviate restenosis.

Graphical Abstract

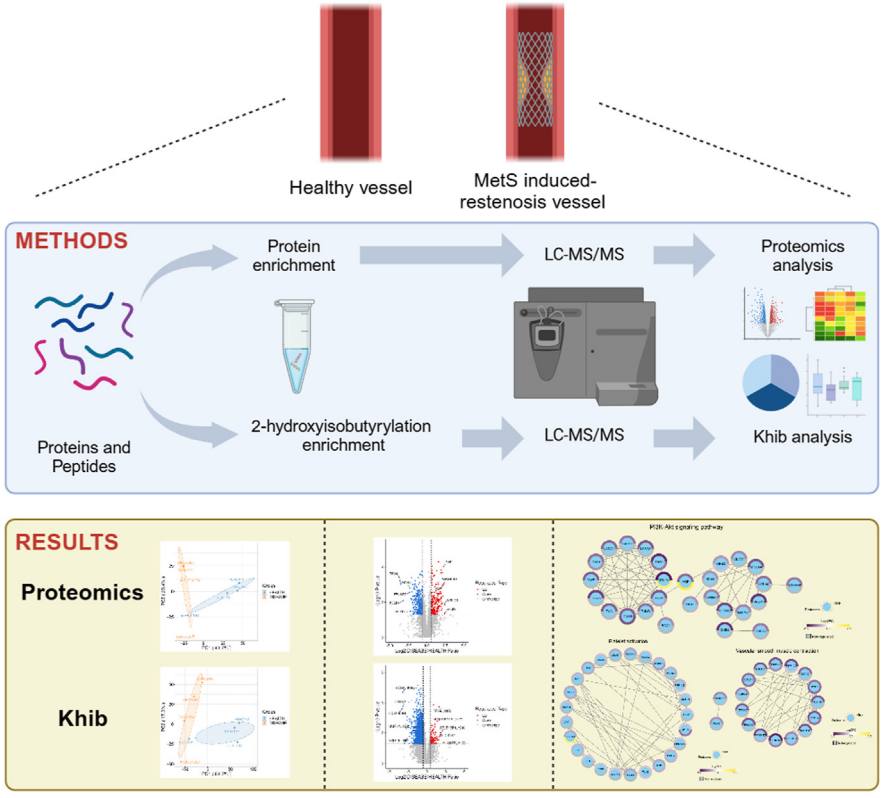

Highlights

- Endovascular neointimal proliferation was significant in patients with MetS-induced restenosis.
- Proteomics and Khib modification omics were performed in the vascular tissues from healthy individuals and patients with MetS-induced restenosis.
- Khib modification differences were significant in pathways related to organic matter metabolism and vascular function.

2025, Mol Cell Proteomics *24*(*6*), 100978
© 2025 THE AUTHORS. Published by Elsevier Inc on behalf of American Society for Biochemistry and Molecular Biology. This is an open access article under the CC BY-NC-ND license (http://creativecommons.org/licenses/by-nc-nd/4.0/).
https://doi.org/10.1016/j.mcpro.2025.100978

Proteomic Analysis and 2-Hydroxyisobutyrylation Profiling in Metabolic Syndrome Induced Restenosis

Xiangyu Liu[1,‡], Liping Zhou[2,3,‡], Wenjing Huang[1], Yanyan Yang[4], Yijun Yang[5], Tianwei Liu[6], Mingjin Guo[1,*], Tao Yu[7,*], and Yongxin Li[1,*]

Restenosis is the primary complication following stenting for coronary and peripheral arterial disease, posing an ongoing clinical challenge. Metabolic syndrome (MetS), characterized by metabolic disturbances, has been identified as an independent predictor for postoperative restenosis in coronary and carotid arteries, potentially due to endothelial dysfunction and augmented oxidative stress in cells, while its specific regulatory mechanism is still largely unknown. Lysine 2-hydroxyisobutyrylation (Khib), a recently identified posttranslational modification, plays a crucial role in transcriptional regulation and cellular metabolism. However, there is a lack of comprehensive analysis of the proteome and Khib modifications within restenotic vessels in the context of MetS, as well as in the understanding of the associated pathophysiology. In this study, we observed a significant upregulation of Khib in restenotic arteries induced by MetS, confirmed by animal and cellular experiments. Further, using high-throughput liquid chromatography-mass spectrometry, we catalogued 15,558 Khib sites across 2568 proteins, implicating a multitude of biological functions. Analysis revealed 2007 Khib sites on 1002 proteins with considerable differential modifications which are present within the cytoplasm and nucleus. Interestingly, proteins located in the mitochondria, endoplasmic reticulum, and cell membrane also exhibit distinct expression and modification profiles to varying extents that related to vascular smooth muscle contraction, platelet activation, and the PI3K-Akt signaling pathway. Notably, the level of COL1A1 protein detected in the protein–protein interaction pathway network and the level of Khib modification are diametrically opposed, suggesting a significant role in the disease's pathogenesis. This study provides the first comprehensive proteomic and Khib modification overview of MetS-related in-stent restenosis vasculature, offering key insights to inform novel therapeutic approaches for restenosis mitigation.

Peripheral artery disease is a prevalent condition associated with high morbidity and mortality. It can cause limb amputation and severely reduce quality of life (1–3). Current treatment of symptomatic peripheral arterial disease is predominantly through endovascular therapy, which utilizes guidewires, catheters, and advanced technologies such as drug-eluting devices, specialized balloons, and biomimetic stents (4–6). However, in-stent restenosis (ISR) remains a significant drawback, typically manifesting as recurrent occlusion symptoms within 3 to 6 months post procedure (7, 8). Metabolic syndrome (MetS) encompasses a cluster of conditions, such as dyslipidemia, inflammation, insulin resistance, and hypertension, which heighten the risk of obesity, diabetes, and cardiovascular diseases. Research indicates that individuals with MetS are at a 3 to 10-fold increased risk for atherosclerotic vascular disease compared to the nonaffected population (9). Hypertension (10), hyperlipidemia (11–14), and hyperglycemia (15, 16) are significantly associated with an elevated risk of stent failure driven by ISR. Thus, metabolism is widely considered to play a crucial role in the development of ISR; however, the precise mechanisms remain to be virtually unknown (17, 18).

Posttranslational modifications (PTMs) dynamically regulate protein function by adding or removing amino acid residues or other chemical groups after synthesis (19–21). PTMs, such as phosphorylation, acetylation, lactylation, succinylation, and ubiquitylation, are reported to be critical in modulating cardiovascular pathophysiology (22–26). The 2-hydroxyisobutyrylation (Khib) modification, identified by Dai *et al*. in 2014, is a conserved PTM linked to various biological functions,

From the [1]Department of Vascular Surgery, The Affiliated Hospital of Qingdao University, Qingdao, Shandong, PR China; [2]School of Optometry, The Hong Kong Polytechnic University, Kowloon, Hong Kong SAR, PR China; [3]Department of Applied Biology and Chemical Technology, The Hong Kong Polytechnic University, Kowloon, PR China; [4]Department of Immunology, School of Basic Medicine, Qingdao University, Qingdao, Shandong, PR China; [5]Archives Department, The Affiliated Hospital of Qingdao University, Qingdao, Shandong, PR China; [6]Medical Research Center, the Affiliated Hospital of Qingdao University, Qingdao, Shandong, PR China; [7]Institute for Translational Medicine, The Affiliated Hospital of Qingdao University, Qingdao, Shandong, PR China

‡These authors contributed equally to this work.

*For correspondence: Mingjin Guo, qduahvasc@163.com; Tao Yu, yutao0112@qdu.edu.cn; Yongxin Li, alexander1985827@163.com.

© 2025 THE AUTHORS. Published by Elsevier Inc on behalf of American Society for Biochemistry and Molecular Biology.
This is an open access article under the CC BY-NC-ND license (http://creativecommons.org/licenses/by-nc-nd/4.0/).

https://doi.org/10.1016/j.mcpro.2025.100978

including metabolism and pathogenesis (27). Recent studies reveal that Khib modification also plays a role in glycolysis, psoriasis, cancer progression, and sperm motility (28–33). For instance, when P300 is deleted as a lysine 2-hydroxyisobutyryltransferase, the levels of Khib at specific sites on crucial glycolytic enzymes that are dependent on P300 are significantly reduced. Consequently, this reduction leads to a decrease in their catalytic activity. It has been observed that Khib also plays a role in regulating energy metabolism, including processes like the citric acid cycle, fatty acid metabolism, and pyruvate metabolism. These findings suggest that Khib may potentially contribute to the regulation of diseases related to metabolism. (28, 34). Therefore, the specific effects of Khib on the cardiovascular system, particularly peripheral vessels, require further investigation.

Here, we firstly validate changes in expression and distribution of Khib in vascular tissues in clinical tissue and cell models. Subsequently, we utilized proteomics and PTMomics to examine the protein and Khib modification characteristics in MetS-induced restenosis. Functional enrichment analysis revealed a marked decrease in Khib sites related to smooth muscle cell contraction, PI3K-AKT signaling, and platelet activation. Conversely, there was an increase in Khib sites linked to HIF-1 signaling, lipid metabolism, and atherosclerosis, underscoring specific sites within these pathways with notable disparities. These results validate the hypothesis that modifications at the Khib site might be closely related to the specific functions of these proteins, subsequently influencing the pathogenesis and progression of restenosis associated with metabolic syndrome.

EXPERIMENTAL PROCEDURES

Experimental Design and Statistical Rationale

This study was approved by the Medical Research Ethics Committees of the Affiliated Hospital of Qingdao University (QYFYWZLL29069). All individuals provided written consent for the collection of samples, their analysis, and the disclosure of their fundamental and clinicopathological data. Specimen acquisition occurred at the Vascular Surgery and Organ Transplantation Unit, categorizing them into normal (n = 10) and pathological (n = 10) cohorts for this investigation. The current report identifies specific features of metabolic syndrome, which include elevated blood pressure (≥130/85 mm Hg), low levels of high-density lipoprotein cholesterol (<40 mg/dl [1.0 mmol/L] for men and <50 mg/dl [1.3 mmol/L] for women), high triglyceride levels (≥150 mg/dl [1.7 mmol/L]), and hyperglycemia (fasting glucose ≥100 mg/dl [6.1 mmol/L]) (35). The presence of at least 3 out of the 4 traits is indicative of the metabolic syndrome. Four samples from each group were randomly selected for subsequent omics study. Preexperimental patient data encompassing serology and imaging were compiled. Each cohort provided triplicate biological replicates for subsequent proteomic and Khib-modified omics scrutiny. Data quality assurance for omics outputs was verified using statistical tools like Pearson's correlation coefficient, principal component analysis, and relative standard deviation. Statistical significance was determined through Student's *t* test, with *p* values below 0.05.

Rat Carotid Artery Balloon Injury Model

All animal experiments conducted in this study were granted ethical approval by the Experimental Animal Ethics Committee of the Medical Department at Qingdao University (20230625Wistar1220230901177). The procedures adhered to the guidelines outlined in the National Institutes of Health Guide for the Care and Use of Laboratory Animals. Rat carotid artery injury was induced as described previously (36). Wistar male rats, 8 weeks of age, obtained from Beijing Vital River Laboratory Animal Technology Co, Ltd, were subjected to experimental procedures under anesthesia induced by pentobarbital sodium (50 mg/kg, i.p.). A ventral cervical incision was performed to reveal the left common carotid artery and its proximal segment. The external carotid artery was incised, and a 2F Fogarty catheter was introduced. Upon inflation of the catheter's balloon to 1.5 atm, endothelial damage was induced via reciprocal motion. The procedure concluded with ligation of the external carotid artery, reestablishing perfusion in the common carotid artery.

Vascular Morphological Evaluation and Modification Localization

Immunohistochemistry (IHC) staining analysis was performed as previously reported (37). The vascular specimens were preserved in a 4% solution of formaldehyde for 3 to 5 days, followed by ethanol dehydration for subsequent paraffin embedding and sectioning. Sections of 6 μm thickness were prepared and subjected to H&E staining. Digital images of these sections were captured at 40x magnification. Identical preparation processes were employed for sections designated for IHC. These paraffin-embedded sections underwent dewaxing and rehydration, then were treated with 0.3% hydrogen peroxide for 30 min to quench endogenous peroxidase activity. Antigen retrieval was conducted using 0.1 M EDTA, pH 6.0, for 15 min. After blocking with normal serum, the sections were incubated with anti-2-hydroxy-isobutylated lysine primary antibody (PTM802, 1:1000 dilution, PTM Biolab) followed by a biotinylated secondary antibody. Visualization was achieved using an avidin-biotin complex coupled with peroxidase and 3,3′-diaminobenzidineas the chromogen. Finally, the sections were counterstained with H&E.

Western Blot

The proteins derived from the vascular tissues of both individuals with and without diseases were separated using SDS-PAGE technique. Subsequently, these proteins were immobilized onto a polyvinylidene fluoride membrane (Millipore, America) with a pore size of 0.22 μm. To prevent nonspecific binding, a blocking step was performed by incubating the membrane in Tris-Buffered Saline with Tween 20 containing 5% nonfat milk at room temperature for 1 hour. The membrane was then subjected to overnight incubation at 4 °C with an anti-2-hydroxy-isobutylated lysine antibody (PTM802 1:1000; PTM Biolab), followed by an one-hour incubation at room temperature with a secondary antibody specific to mouse IgG (H + L) (Pierce). Detection of protein bands on the membrane was achieved using an advanced electrochemiluminescence system (apparatus: Chemiluminescent Imaging).

Proteome and Khib PTM Omics Procedures

Protein Extraction—The sample was obtained from a storage at −80 °C, measured in weight, crushed using liquid nitrogen as a freezing agent, and then transferred into a centrifuge tube with a capacity of 5 ml. Then, the volume of pulverized tissue in cracking buffer (consisting of 1% Triton X-100, 1% protease inhibitor cocktail, 3 μM trichostatin A, and 50 mM nicotinamide) was increased fourfold. The mixture underwent sonication for a duration of 3 min while placed in an ice-water bath using a high-intensity ultrasonicator manufactured by Scientz. Subsequently, the sample was subjected to centrifugation at

a speed of 12,000*g* for a period of 10 min at a temperature of 4 °C. The resulting pellet was discarded, and the supernatant was collected for protein quantification utilizing the bicinchoninic acid assay following the provided protocol.

Trypsin Digestion—In the beginning, an equal amount of chilled acetone was mixed with the protein sample, followed by adding four times that volume of acetone to induce precipitation at a temperature of −20 °C for a duration of 2 h. After precipitation, the sample underwent centrifugation at 4500*g* for 5 min. The liquid above the sediment was discarded, and the solid residue was rinsed with cold acetone 2 to 3 times before being dried. Subsequently, the solid residue was dissolved again in tetraethylammonium bromide (TEAB) solution with a concentration of 200 mM and subjected to sonication for dispersion. Proteolytic digestion was performed overnight using trypsin at a ratio of one part protease to 50 parts protein. Reduction of the samples was performed at 56 °C using 5 mM DL-DTT for 30 min, followed by alkylation with 11 mM iodoacetamide in the dark at room temperature for 15 min.

Khib-modified Affinity Enrichment—To concentrate the modified peptides, they were solubilized in immunoprecipitation buffers and centrifuged to discard any insoluble material. The clear supernatant was then incubated with precleaned resin on an orbital shaker at 4 °C overnight. Subsequent washes included four cycles with immunoprecipitation buffer followed by two cycles with deionized water. The peptides attached to the resin were eluted in three distinct stages using trifluoroacetic acid at a concentration of 0.1%. The eluates obtained from each step were combined and subjected to lyophilization. To prepare for liquid chromatography-tandem mass spectrometry analysis, the resulting peptides underwent desalting utilizing C18 ZipTips (Millipore) as per the manufacturer's guidelines.

Liquid Chromatography-Tandem Mass Spectrometry

In a custom-built reverse-phase column (25 cm × 100 μm), the peptide dissolved in mobile phase A was directly introduced. The separation utilized a binary solvent system: solvent A (0.1% formic acid in 2% acetonitrile/water) and solvent B (0.1% formic acid in acetonitrile), following a gradient elution program: initially 6%-22% solvent B over 40 min, then 22%-30% solvent B from 40 to 52 min, proceeding to 30%-80% solvent B between 52 and 56 min, and holding at 80% solvent B for the final 4 min, at a flow rate of 450 nl/min. Ultra-high performance liquid chromatography with a capillary ionization source facilitated the separation before analysis by timsTOF Pro2 mass spectrometry. The ion source was set to 1.6 kV. The analysis of mass-to-charge (m/z) was conducted using a time-of-flight detector in tandem mass spectrometry (MS/MS) mode, utilizing parallel accumulation-serial fragmentation technology. The range of m/z analyzed was 100 to 1700. Our focus was on ions with charge states ranging from 0 to 5. Each cycle included 10 parallel accumulation-serial fragmentation MS/MS scans, and we implemented a dynamic exclusion period lasting for 24 s. Raw data for all proteomics and 2-Khib modiomics generated by MaxQuant have been uploaded to the ProteomeXchange Consortium *via* the PRIDE (38) partner repository with the dataset identifier PXD062384, and annotated spectra for identified proteomics and Khib modifications have been deposited on MS-viewer with the search key "4xxtqp3gqg" and "kc21vnele4".

Data Search—The MS/MS datasets were processed using MaxQuant software version 1.6.15.0. A *Homo sapiens* reference proteome (Homo_sapiens_9606_SP_20230103.fasta with 20,389 sequences) was used for matching peptide sequences, along with a reverse decoy and contaminant database. The designated protease was Trypsin/P, allowing for up to two missed cleavages. Peptides had to be at least seven amino acids long and could have a maximum of five modifications. Both precursor and fragment ions had a mass tolerance of 20 ppm in the initial and main searches. Cysteine residues were fixedly modified by carbamidomethylation, while protein N-terminal acetylation, methionine oxidation, and 2-hydroxyisobutyrylation were considered as variable modifications. To ensure stringent control, the false discovery rate for protein identification, peptide validation, and peptide-spectrum match was maintained below 1%.

Data Analysis—The significance of the overrepresentation of differentially expressed proteins (DEPs) was determined using Fisher's exact test, focusing on the proteins that were identified. Functional categories exhibiting an enrichment fold change greater than 1.5 and a p value less than 0.05 were considered statistically significant.

Bioinformatics Analysis—Functional annotation of identified proteins was conducted by extracting Gene Ontology (GO) identifiers via eggNOG-Mapper, referencing the eggNOG database. This process enabled categorization into cellular components, molecular functions, and biological processes. The Kyoto Encyclopedia of Genes and Genomes (KEGG) amalgamates data on protein interactions, including pathway networks, genes, biological complexes, and chemical reactions. Proteins were mapped to KEGG pathways using BLAST (blastp, value≤1e-4) and annotated based on the highest-scoring alignment. In eukaryotic cells, protein localization varies with membrane affinity, occupying structures such as the extracellular matrix, cytoplasm, nucleus, and organelles like mitochondria, the Golgi apparatus, and endoplasmic reticulum (ER). WoLF PSORT was utilized to predict and annotate these proteins' subcellular localizations. For the protein interaction network, the STRING database facilitated the identification of disease-relevant interactions among DEPs within KEGG pathways, assigning a high confidence score of 0.7 to these relationships.

Statistical Analysis—Proteomic and Khib-modified omic profiles were analyzed in vascular specimens from quartets of subjects per cohort, employing relative standard deviation, principal component analysis, and Pearson correlation to evaluate reproducibility. Statistical significance of disparities was determined using t tests, while GraphPad Prism 8 facilitated graphical representation. Significance was denoted by p values lower than 0.05.

RESULTS

Clinical Characteristics of the Study Groups

Clinical data indicated normative cardiovascular and metabolic parameters in the control cohort, in contrast to the disease cohort which presented with dyslipidemia, hyperglycemia, hypertension, or had a diagnosis of MetS (Fig. 1*A* and Table 1). These findings highlight the increased risk of atherosclerotic vascular diseases in MetS patients, due to disrupted glucose and lipid homeostasis. Enhanced computed tomography imaging depicted significant femoral artery occlusions and lumen narrowing among restenosis subjects (Fig. 1*B*).

Morphological Analysis and Khib Distribution of Human and Rat Vessels

Prior studies have demonstrated a significant correlation between restenosis following vascular injury and the proliferation of endothelial cells, leading to neointimal formation (39, 40). Histological analyses via H&E staining confirmed these findings by demonstrating luminal narrowing and vessel wall thickening in both healthy and restenotic vascular tissues (Fig. 2, *A* and *B*). A focused examination of Khib modifications within restenotic vasculature revealed a pronounced

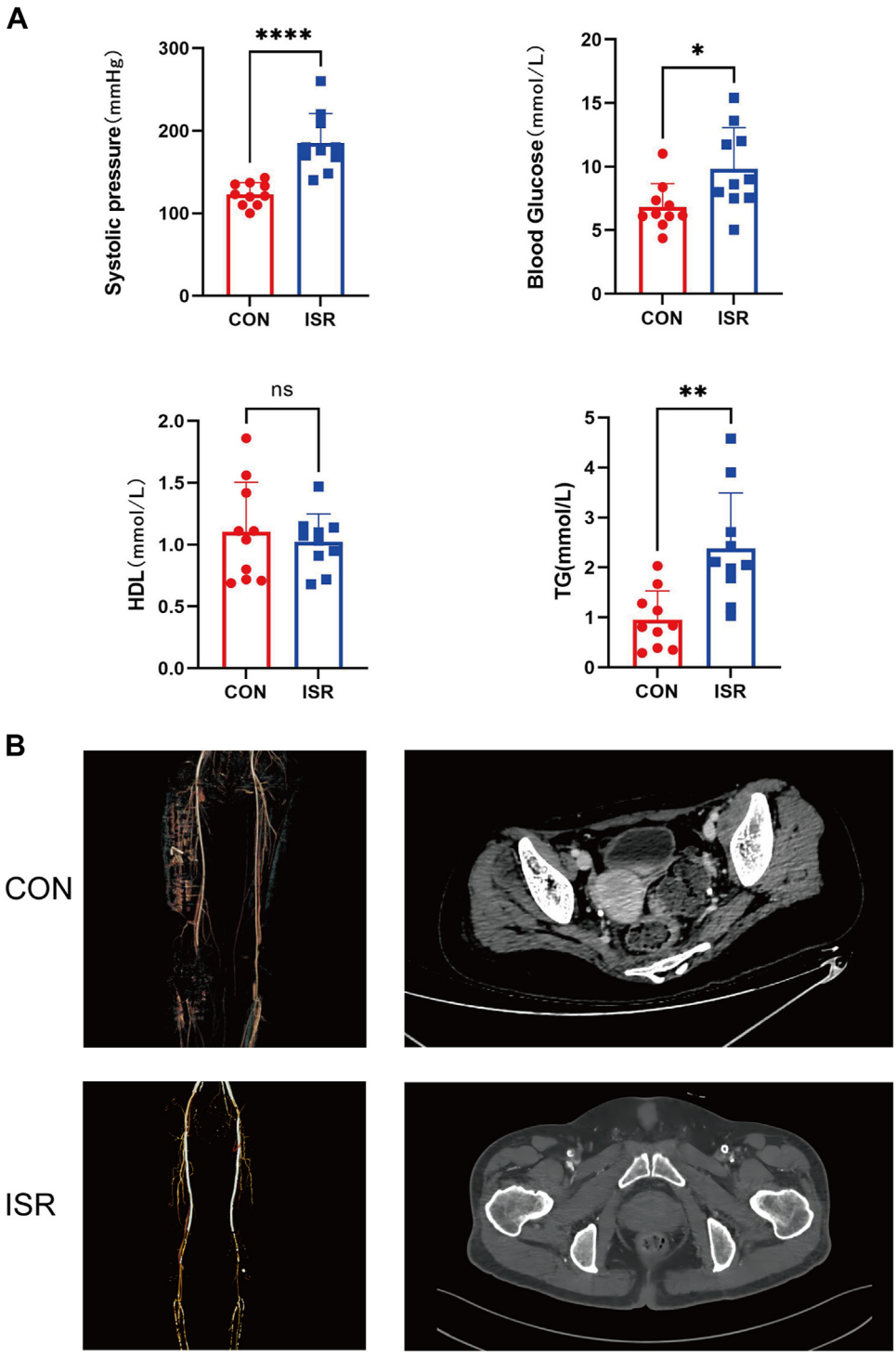

FIG. 1. **Clinical characteristics in clinical patients.** *A*, serological indicators in clinical patients; *B*, computed tomography angiography (CTA) in clinical patients. Data are presented as mean ± SD. n = 10 per group. *$p < 0.05$, **$p < 0.01$, ****$p < 0.0001$.

expression across all vascular layers, with a notably reduced presence in the intima of restenotic vessels compared to healthy counterparts. In the development of ISR, endothelial cell regeneration and proliferation post mechanical stimulation are pivotal mechanisms. Our group's prior research indicated distinct Khib modification patterns in MetS patients with ISR, with endothelial differentiation being the obvious different. Western blot analysis of clinical samples revealed a significant

TABLE 1
Patient clinical characteristics

Group	Number	Blood pressure (mmHg)	Triglyceride (mmol/L)	High-density lipoproteincholesterol (mmol/L)	Fasting blood glucose (mmol/L)
Healthy	1	123/81	1.28	1.56	6.29
Healthy	2	133/68	1.67	1.11	7.36
Healthy	3	137/79	1.14	0.72	5.44
Healthy	4	143/86	2.03	0.71	6.16
Healthy	5	110/80	0.81	0.8	6.95
Healthy	6	135/87	0.84	1.42	6.11
Healthy	7	121/72	0.35	1.86	11.03
Healthy	8	100/79	0.71	1.11	4.37
Healthy	9	120/76	0.29	0.69	6.1
Healthy	10	110/67	0.39	1.04	8.39
Disease	1	168/91	2.05	1.07	5.04
Disease	2	148/75	1.03	1.1	7.56
Disease	3	209/112	1.98	1.47	11.74
Disease	4	140/85	3.9	0.95	15.4
Disease	5	180/110	1.2	1.14	8
Disease	6	170/111	1.78	0.68	7.5
Disease	7	176/92	2.71	10.3	8.6
Disease	8	220/110	4.58	0.72	12
Disease	9	260/100	2.11	1.15	13.6
Disease	10	180/98	2.43	0.91	9

Abbreviations: FBG, fasting blood glucose; HDL-C, high-density lipoproteincholesterol; TG, triglyceride.

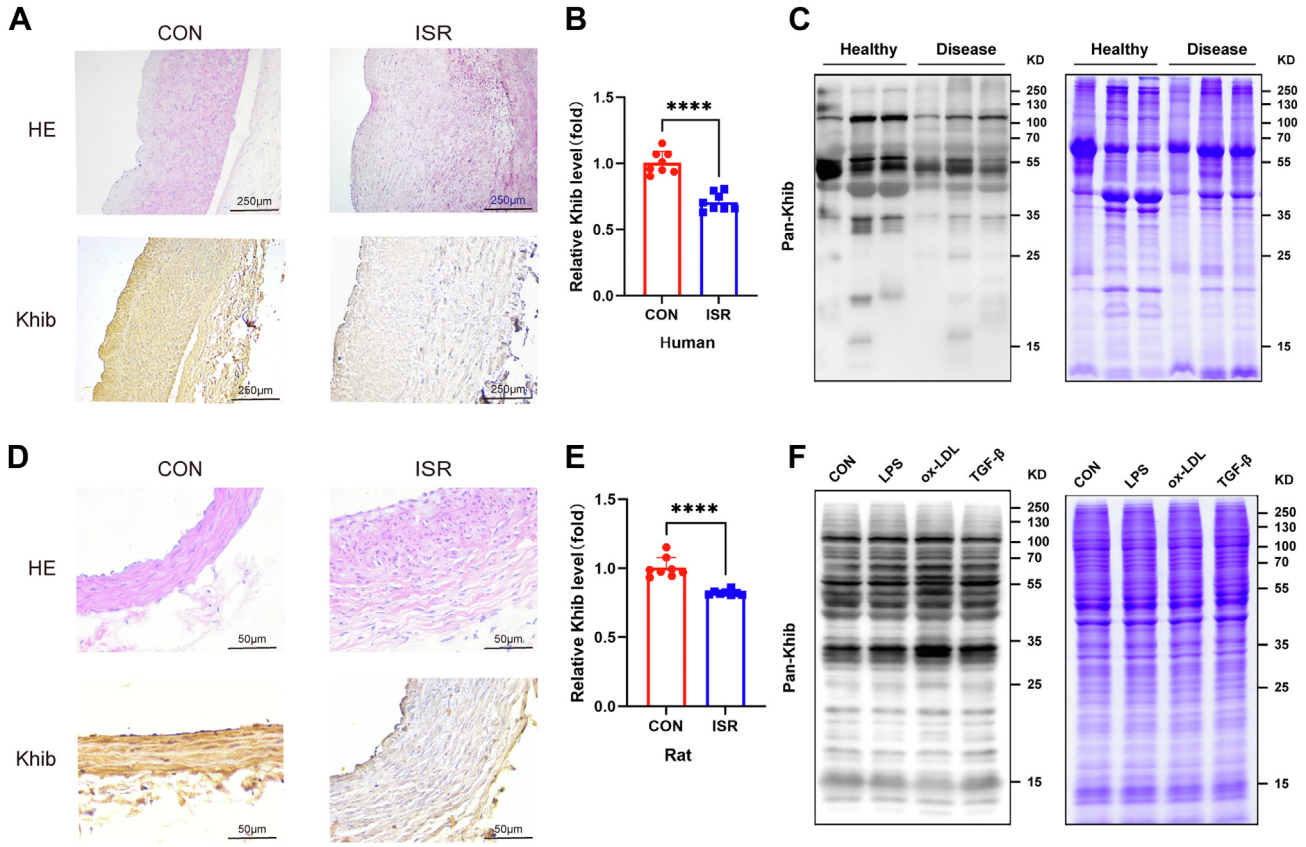

FIG. 2. **Vascular morphological characteristics in clinical and animal samples.** *A*, H&E and Khib immunohistochemical staining from healthy and in-stent restenosis clinical samples. The *red scale* indicates a length of 250 μm. *B*, quantitative analyses of A; *C*, WB analysis of Khib in clinical samples. *D*, H&E and Khib immunohistochemistry of healthy and carotid balloon injury rats. The *red scale* indicates a length of 50 μm. *E*, quantitative analyses of D; *F*, HUVEC cells were treated with LPS, ox-LDL, and TGF-β, respectively, for 24 h. Data are presented as mean ± SD. $^{*}p < 0.05$, $^{**}p < 0.01$. LPS, lipopolysaccharide; ox-LDL, oxidized low-density lipoprotein; TGF-β, transforming growth factor-beta; WB, western blot.

reduction in Khib modification across various proteins, particularly ranging from 25 to 110 kDa in patient samples compared to healthy controls. (Fig. 2*C*). This pattern was consistently observed in carotid artery balloon injury rat models which was used to mimic post injury restenosis (Fig. 2, *D* and *E*), suggesting a potential link between diminished Khib modification and intimal alterations in MetS patients with restenosis. Moreover, the vascular endothelium functions as a semipermeable barrier, and impaired reendothelialization is the primary cause of elevated ISR risk (41). By treating endothelial cells with various stimulators such as lipopolysaccharides, oxidized low-density lipoproteins, and tumor necrosis factor alpha, we observed a significant downregulation of Khib levels specifically under transforming growth factor-beta stimulation, with only a slight decrease under other conditions (Fig. 2*F*), implying Khib might play roles in specific environment which need deeper investigation.

Proteomic Profiling and Functional Insights

Label-free proteomic quantification is an advanced technique that quantifies proteins without relying on isotope labeling (42). Four-dimensional proteomics introduces ion mobility separation as an additional dimension to the traditional 3D framework, which includes retention time, mass-to-charge ratio (m/z), and ion intensity (43). To identify protein biomarkers for MetS and restenosis, we conducted a comparative 4D label-free quantitative proteomic analysis on liver vessel and femoral artery samples from both healthy individuals and those affected by the aforementioned conditions (n = 4 per group). Our analysis yielded quantification results for 3768 proteins across the vascular tissues under study (Fig. 3, *A* and *B*, and Supplemental Table S1). We conducted quality control assessments of peptide length distribution, peptide number distribution, protein coverage distribution, and protein molecular weight distribution to ensure result quality (Fig. 3, *C–F*). Pearson's correlation coefficient, principal component analysis, and relative standard deviation confirmed the consistency of quantitative results across biological and technical replicates. (Fig. 3, *G–I*). Applying a cutoff of 1.5-fold change and a statistical significance threshold of $p < 0.05$, we discerned 469 proteins exhibiting differential expression: 281 were significantly downregulated, while 188 were upregulated (Fig. 4*A* and Table 2). Among the notably altered proteins, those downregulated were found in the plasma membrane, nucleus, and mitochondria, whereas upregulated proteins were located in the plasma membrane, cytoplasm, and extracellular. Notably, APOO, a gene involved in lipid transport and metabolism, exhibited marked downregulation (44). Conversely, the upregulated protein hepatocyte growth factor plays a role in angiogenesis and tissue regeneration (45). These variances in protein expression may be linked to the pathogenesis of MetS-induced restenosis.

To elucidate the functional profiles of DEPs, we first analyzed the subcellular localization. We simultaneously contrasted the profiles of upregulated *versus* downregulated DEPs. DEPs mainly locate in the cytoplasm (143, 30.49%) and nucleus (119, 25.37%), with substantial numbers also present in the extracellular space (85, 18.12%) and mitochondria (43, 9.17%) (Fig. 4*B*). At the same time, GO enrichment highlighted “regulation of biological process” and “cellular component organization or biogenesis” as the predominant biological processes (Fig. 4*C*). DEPs were primarily associated with intracellular structures and cytoplasm in the cellular component category, while “protein binding” and “ion binding” were the most represented molecular functions. Furthermore, Clusters of Orthologous Groups/Eukaryotic Orthologous Groups (COG/KOG) analysis revealed a notable prevalence of DEPs in cellular processes and signaling, especially in signal transduction mechanisms and cytoskeletal components (Fig. 4*D*). Notably, metabolic proteins comprised about 18% of the DEPs, with subsets dedicated to energy production and conversion (17/461), lipid transport and metabolism (14/461), and carbohydrate transport and metabolism (13/461) being notably represented. To assess the variation in protein function enrichment among DEPs, a KEGG pathway analysis was conducted. This analysis identified the key pathways involved in disease's pathogenesis (Fig. 4*E*). The results indicated that pathways involving focal adhesion, platelet activation, and vascular smooth muscle contraction are significantly implicated in the DEPs associated with the disease.

Characterization of Differentially Modified Khib Proteins

In order to elucidate the impact of Khib modification on disease progression, we conducted a proteomic analysis contrasting healthy and pathological tissue samples. Evaluations of quality control and reproducibility, including peptide length distribution, Pearson correlation coefficient, principal component analysis, and relative standard deviation, confirmed that the results satisfied the required quality and statistical standards (Fig. 5). The analysis revealed 2007 statistically significant Khib modification sites across 1002 proteins. These modifications displayed variable distribution, with 1108 sites exhibiting a singular alteration, while 672 proteins harbored in excess of 10 modifications, suggesting a complex relationship between protein function and modification patterns (Figs. 3*B*, 6*A*, and Supplemental Table S2). Specifically, within the context of MetS induced ISR, a substantial downregulation of Khib sites occurred in 1922 sites across 926 proteins, in stark contrast to only 85 upregulated sites across 76 proteins (Fig. 6*B*). A radar chart was constructed to depict the comparative expression of the top 30 modified sites (Fig. 6*C* and Table 3). Notably, HSPA9 K368 and PRDX2 K10 exhibited significant differences among the protein Khib modification, suggesting their regulatory capacity could be modulated *via* Khib

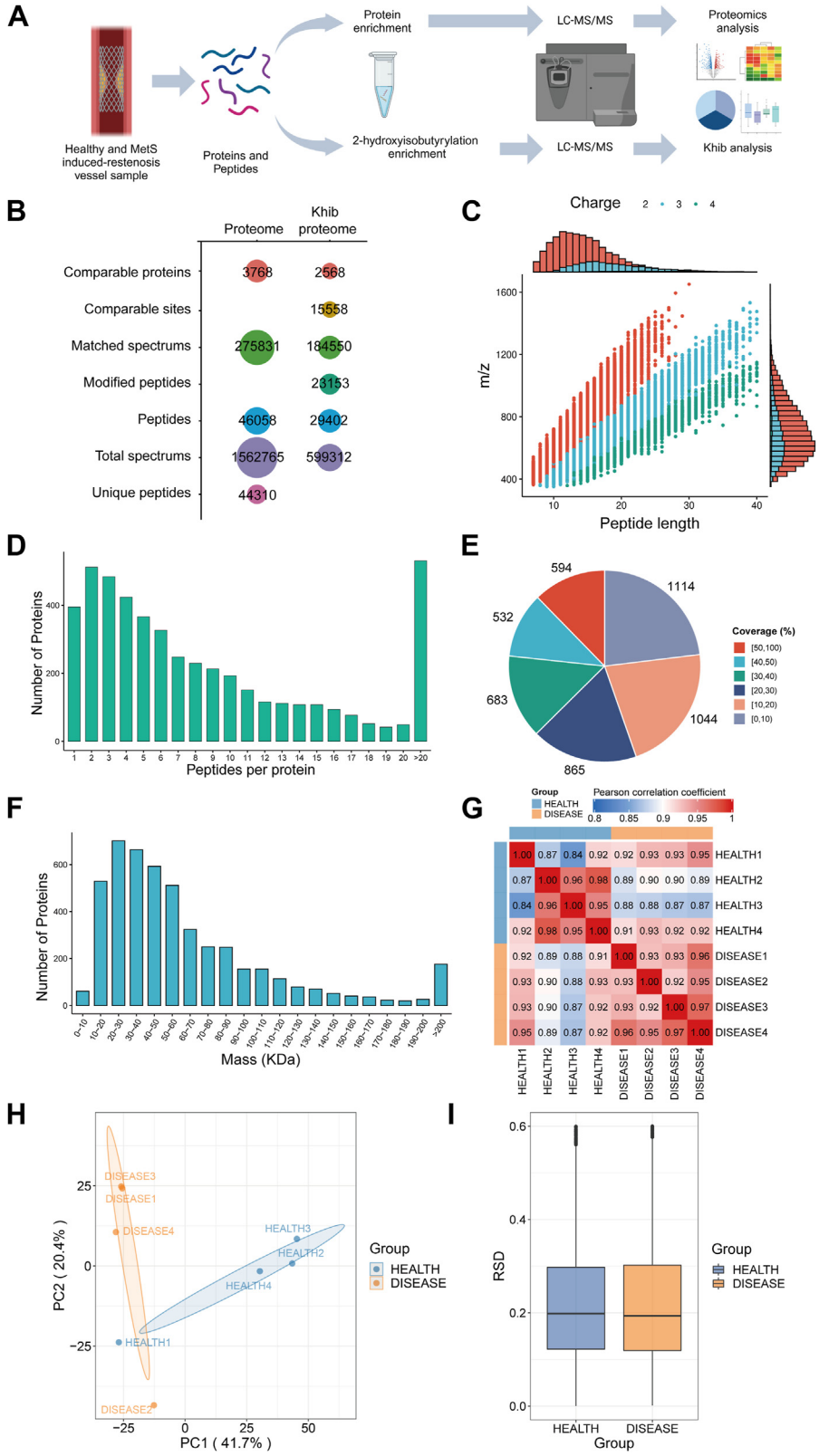

FIG. 3. **Proteomics sample quality control.** *A*, flow diagram of proteomics and Khib modification of tissue from clinical samples of healthy and MetS patients with restenosis; *B*, overview of proteomics and modification; *C*, peptide length distribution; *D*, number distribution of peptides; *E*, protein coverage distribution; *F*, molecular weight distribution of protein; *G*, principal component analysis; *H*, Pearson's correlation coefficient; *I*, relative standard deviation. MetS, metabolic syndrome.

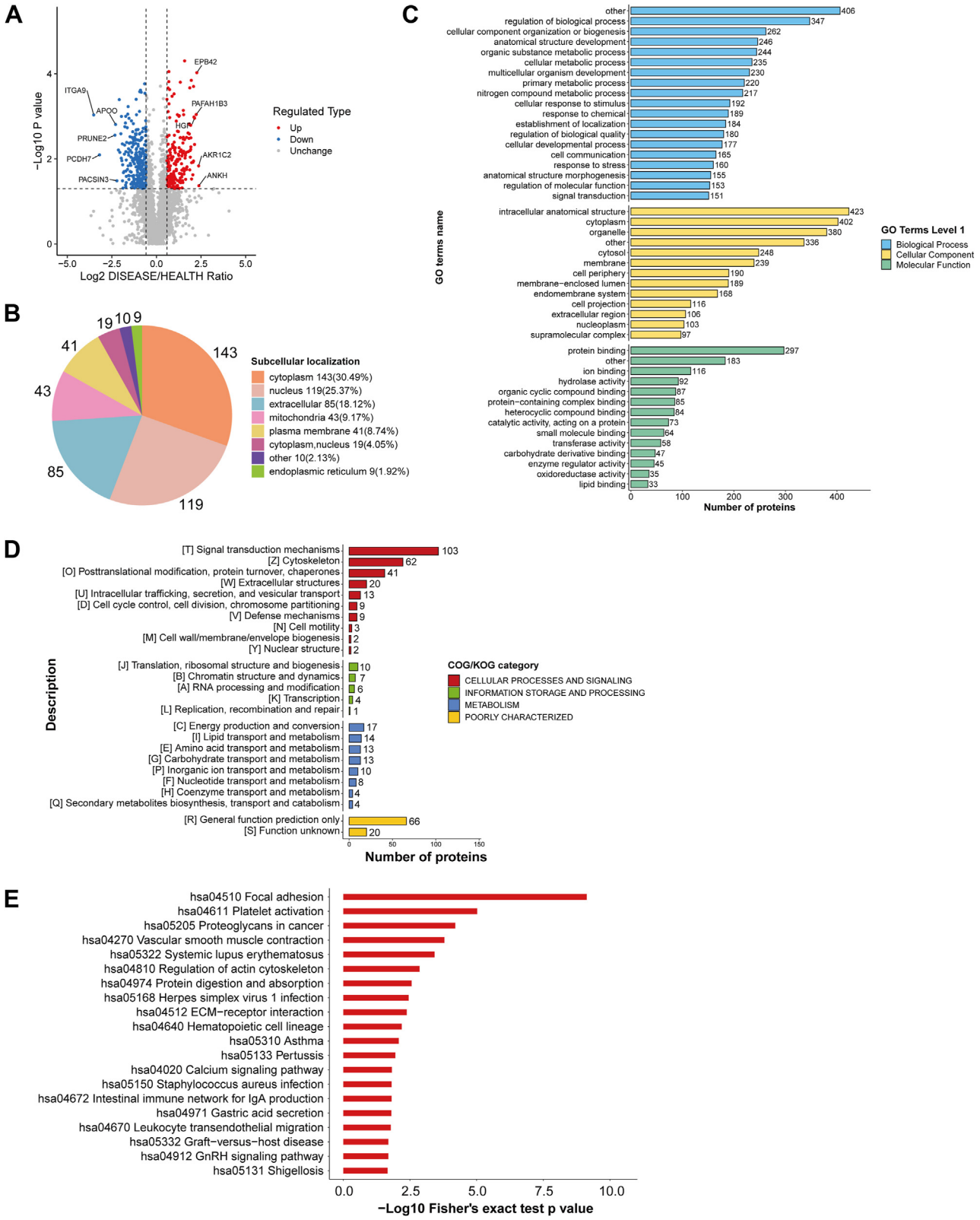

FIG. 4. **Whole proteomics analysis of healthy and diseased vessels.** *A*, volcanic map of DEPs, *blue* indicates downregulated protein, *red* indicates upregulated protein, *gray* indicates no significant difference in protein level; *B*, protein subcellular localization of DEPs; *C*, GO classification of DEPs; *D*, COG/KOG classification of DEPs; *E*, KEGG path analysis of DEPs. COG/KOG, Clusters of Orthologous Groups/Eukaryotic Orthologous Groups; DEPs, differentially expressed proteins; GO, Gene Ontology; KEGG, Kyoto Encyclopedia of Genes and Genomes.

TABLE 2
Comparative expression of top five downregulated and upregulated proteins

Gene name	Disease/Health ratio	Disease/Health *p* value	Regulated type	Subcellular localization
ITGA9	0.087276215	0.000925934	Down	plasma membrane
PCDH7	0.109286045	0.008054663	Down	plasma membrane
PRUNE2	0.199031584	0.002766792	Down	nucleus
APOO	0.204158834	0.00155585	Down	mitochondria
PACSIN3	0.21485538	0.03270773	Down	nucleus
ANKH	5.202782572	0.042833488	Up	plasma membrane
AKR1C2	5.146068285	0.014616051	Up	cytoplasm
EPB42	4.79741105	0.000094155	Up	cytoplasm
PAFAH1B3	4.684430819	0.0009077	Up	extracellular
HGF	4.398681857	0.001103853	Up	extracellular

Abbreviation: HGF, hepatocyte growth factor.

modifications, with potential implications for their functional activity.

To investigate disease-associated site-specific modifications, subcellular localization analysis revealed a predominant cytoplasmic distribution (41.4%), followed by nuclear (21.01%) and extracellular localizations (14.73%) (Fig. 6*D*). We analyzed the most significantly different Khib-modified proteins within critical organelles or cellular membrane structures, specifically the mitochondria (Table 4), the ER (Table 5), and the cytoplasmic membrane (Table 6), aiming to identify key

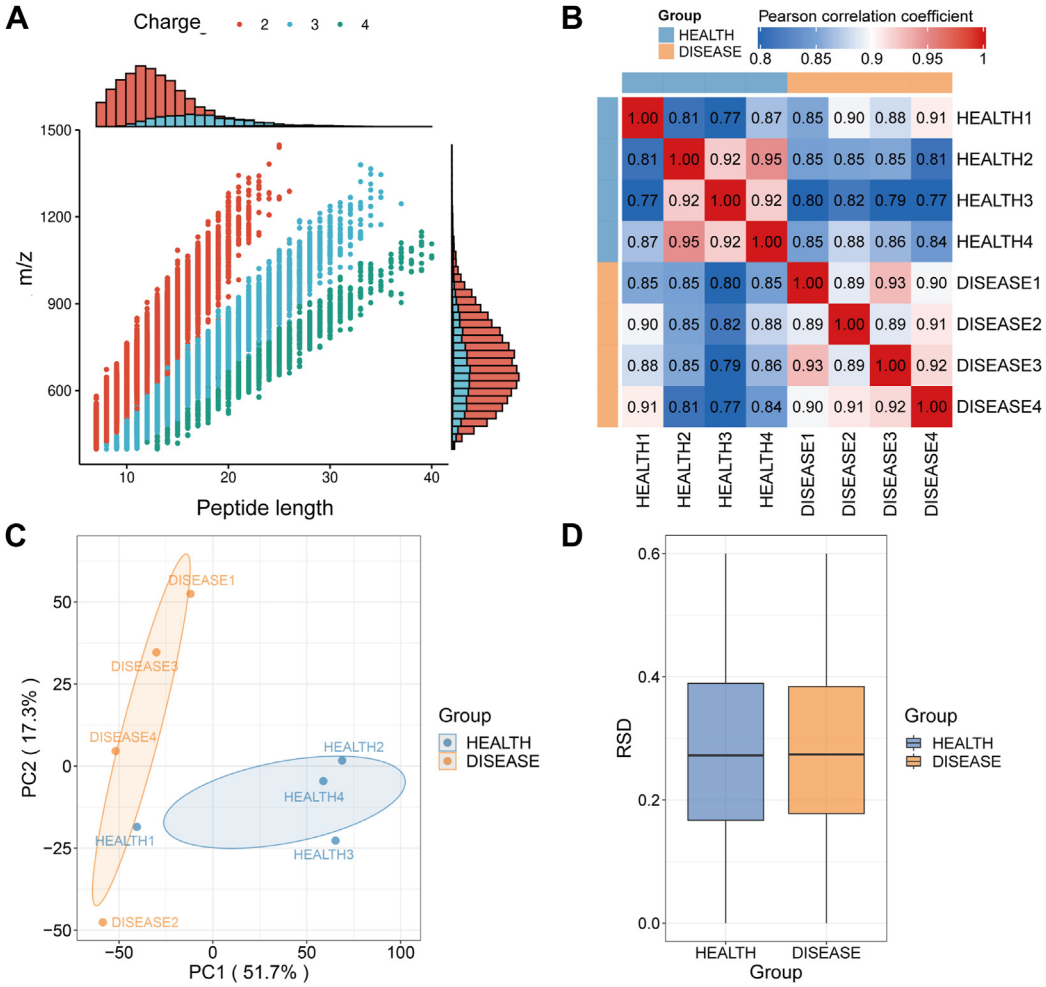

FIG. 5. **2-Hydroxyisobutyrylation sample quality control.** *A*, peptide length distribution; *B*, principal component analysis; *C*, Pearson's correlation coefficient; *D*, relative standard deviation.

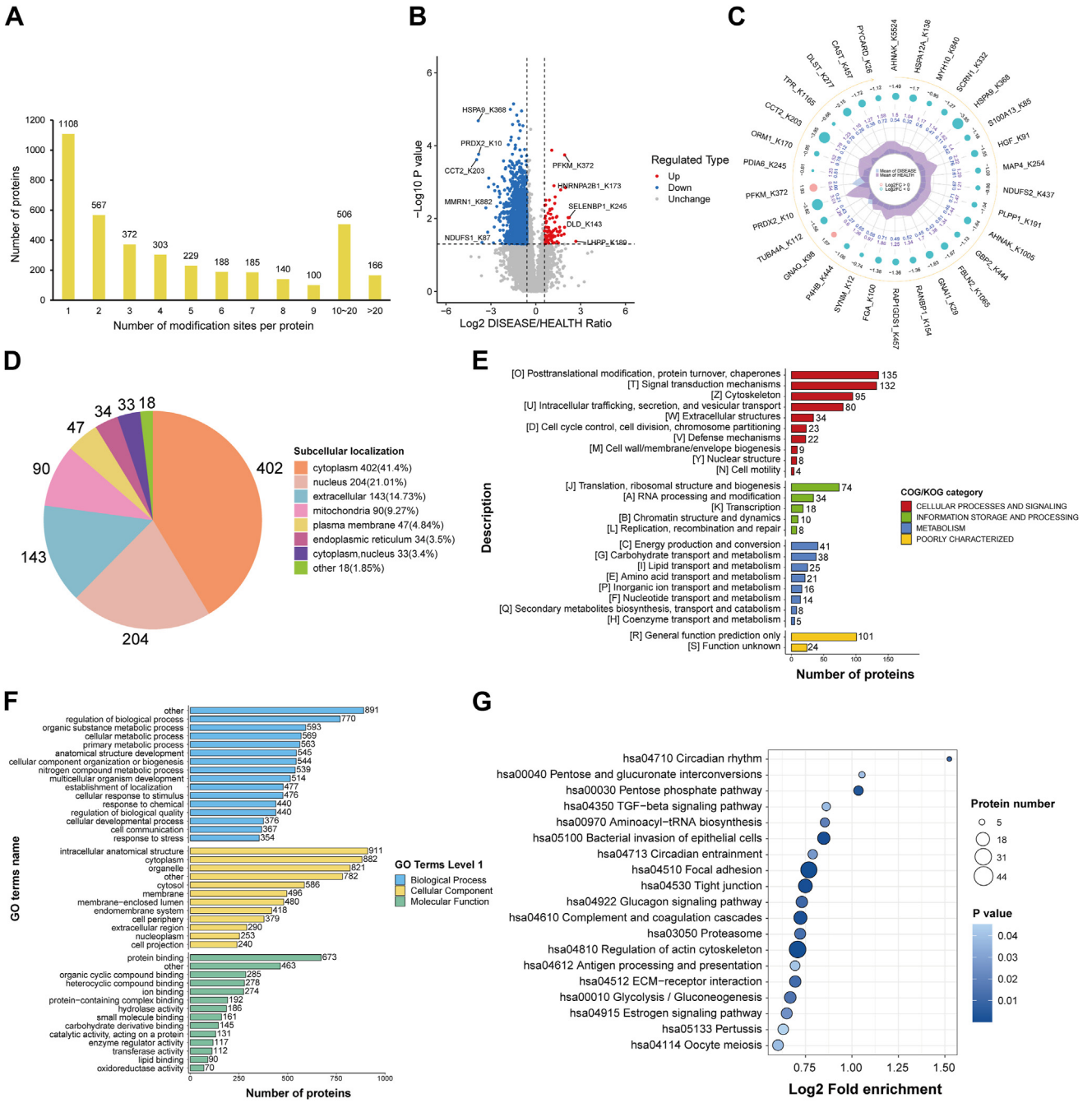

FIG. 6. **Quantitative Khib-modified proteomics in healthy and diseased tissues.** *A*, the quantity distribution of proteins at different Khib modification sites; *B*, volcanic map of Khib modified difference sites; *C*, radar map of top30 Khib modified difference sites; *D*, subcellular distribution of Khib modified proteins; *E*, GO data analysis of Khib modified protein. *F*, COG/KOG functional classification of Khib-modified proteins. *G*, the KEGG pathway was used to analyze Khib differentially modified proteins. COG/KOG, Clusters of Orthologous Groups/Eukaryotic Orthologous Groups; GO, Gene Ontology; KEGG, Kyoto Encyclopedia of Genes and Genomes.

protein modifications that are common across these cellular components and influence cellular composition. Notably, apolipoprotein B exhibits eight significant differential Khib modification sites among ER proteins, with six downregulated (K4465, K273, K1324, K110, K1476, and K2640) and two upregulated (K2340 and K2428) sites (Table 7). Their Khib-modified MS/MS are presented in Supplemental Fig. S1. As a major constituent of low-density lipoprotein, which is strongly associated with cardiovascular conditions like coronary heart disease, elevated levels of apolipoprotein B in the

TABLE 3
Khib comparative expression of the top 30 modified sites

Gene name	Position	Amino acid	Disease	Health	Log2FC	Disease/Health ratio	Disease/Health *p* value
AHNAK	5524	K	0.536	1.501	−1.485	0.357200236	0.000007134
HSPA12A	138	K	0.321	1.041	−1.7	0.307744027	0.000010131
MYH10	840	K	0.605	1.167	−0.949	0.518141302	0.000011135
SCRN1	332	K	0.472	1.141	−1.272	0.414008059	0.000014463
HSPA9	368	K	0.112	1.616	−3.846	0.069556028	0.000020748
S100A13	85	K	0.62	1.404	−1.178	0.442053284	0.000021381
HGF	91	K	0.76	2.224	−1.55	0.341558837	0.000026171
MAP4	254	K	0.606	1.286	−1.086	0.471031895	0.000026637
NDUFS2	437	K	0.669	1.212	−0.858	0.551644961	0.000028338
PLPP1	191	K	0.714	1.465	−1.037	0.487312137	0.000038857
AHNAK	1005	K	0.464	1.443	−1.637	0.321572566	0.000057964
GBP2	444	K	0.609	1.336	−1.133	0.455916422	0.000062816
FBLN2	1065	K	0.431	1.375	−1.673	0.313529061	0.000071121
GNAI1	29	K	0.477	1.697	−1.831	0.280983961	0.000093895
RANBP1	154	K	0.523	1.345	−1.362	0.389063328	0.000096415
RAP1GDS1	457	K	0.488	1.253	−1.359	0.389730511	0.000115366
FGA	100	K	0.713	1.863	−1.385	0.382777644	0.000121896
SYNM	12	K	0.582	0.974	−0.742	0.597819905	0.00012692
P4HB	444	K	0.65	1.355	−1.061	0.479462871	0.000131065
GNAQ	98	K	1.266	0.603	1.069	2.097473461	0.000133411
TUBA4A	112	K	0.426	1.259	−1.562	0.338666911	0.000171128
PRDX2	10	K	0.213	3.012	−3.822	0.070723413	0.000172118
PFKM	372	K	2.059	0.54	1.93	3.810676328	0.000179657
PDIA6	245	K	0.807	1.234	−0.612	0.654302513	0.000187371
ORM1	170	K	0.783	1.518	−0.954	0.516129856	0.000194785
CCT2	203	K	0.116	1.788	−3.951	0.064637914	0.000242225
TPR	1165	K	0.778	1.23	−0.661	0.632324945	0.000261341
DLST	277	K	0.262	1.164	−2.154	0.224692892	0.000261932
CAST	457	K	0.385	1.269	−1.722	0.303214102	0.000262562
PYCARD	26	K	0.725	1.576	−1.119	0.460403783	0.000264149

Abbreviation: HGF, hepatocyte growth factor.

TABLE 4
Regulated Khib sites of mitochondria

Gene name	Position	Amino acid	Disease/Health ratio	Disease/Health *p* value	Regulated type
HSPA9	368	K	0.069556028	0.000020748	Down
NDUFS1	87	K	0.082700936	0.045028215	Down
MMRN1	882	K	0.098923458	0.005061413	Down
DLST	277	K	0.224692892	0.000261932	Down
PPP1R14A	54	K	0.227818019	0.004006594	Down
VCAN	347	K	0.248287168	0.006675348	Down
ALDH4A1	114	K	0.259828855	0.030063667	Down
CS	43	K	0.266387046	0.006422476	Down
GLUD1	527	K	0.275426022	0.039374353	Down
TRAPPC3	156	K	0.275746395	0.007185068	Down
HSPE1	40	K	1.755925943	0.022027751	Up
SARM1	363	K	1.765095397	0.03979646	Up
ATP5F1B	124	K	2.005288855	0.007580275	Up
DES	299	K	2.056049717	0.035361537	Up
ASMTL	306	K	2.145314987	0.023222689	Up
ASMTL	65	K	2.322788598	0.001252511	Up
SOD2	122	K	2.43754217	0.030595323	Up
HSPE1	54	K	2.585565275	0.009214186	Up
DLD	143	K	4.485159971	0.009379678	Up
LHPP	189	K	6.406035927	0.042002532	Up

TABLE 5
Regulated Khib sites of endoplasmic reticulum

Gene name	Position	Amino acid	Disease/Health ratio	Disease/Health *p* value	Regulated type
COL12A1	1324	K	0.208608036	0.048037605	Down
KTN1	337	K	0.232144176	0.007257895	Down
ANPEP	955	K	0.235392071	0.001651932	Down
COL12A1	2384	K	0.236308602	0.000922294	Down
HSP90B1	486	K	0.261859658	0.006836258	Down
ITGA8	141	K	0.329162286	0.030421152	Down
CDH13	185	K	0.334699912	0.008382752	Down
HSP90B1	473	K	0.354897875	0.002642687	Down
BCAP31	190	K	0.368172107	0.000419985	Down
EPHX2	89	K	0.383795889	0.003841767	Down
APOB	2340	K	1.573919855	0.017036071	Up
APOB	2428	K	1.813649847	0.01761469	Up
ITIH1	125	K	1.843558178	0.028314478	Up
HSP90B1	593	K	1.990307946	0.032654082	Up
HSPA5	376	K	1.999596778	0.025754276	Up
FAP	505	K	2.192185698	0.009498326	Up
HSP90B1	97	K	3.273183047	0.028574674	Up
CANX	89	K	3.719318496	0.026629644	Up

APOB, apolipoprotein B.

bloodstream pose a risk for the occurrence of restenosis and reocclusion within the superficial femoral artery among individuals diagnosed with peripheral artery disease (46). These modifications may alter protein structure or function, impacting lipid metabolism pathways. GO analysis highlighted biological process regulation and organic substance metabolism as the primary biological process functions (Fig. 6*E*). Clusters of Orthologous Groups/Eukaryotic Orthologous Groups classifications identified PTMs, protein turnover, chaperoning, and signal transduction as the leading functional groups (Fig. 6*F*). KEGG pathway enrichment analysis displayed that circadian rhythm, the pentose phosphate pathway, and transforming growth factor-beta signaling are associated with Khib modifications (Fig. 6*G*), suggesting these pathways may be involved in protein structural and functional changes contributing to disease pathogenesis.

Characterizing Khib Sites in Human Vessels

To investigate the sequence motifs at modification sites, we utilized the MoMo tool with the MotiF-X algorithm, focusing on the decameric peptide sequences surrounding the targeted sites (Fig. 7*A*). Our analysis indicated a significant enrichment of specific amino acids—alanine (A), aspartic acid (D), glutamic acid (E), isoleucine (I), leucine (L), and valine (V)—at the immediate positions (−1 and +1) adjacent to the Lys Khib sites.

Subsequent to categorizing proteins based on expression fold changes into quartiles Q1 (<0.5), Q2 (0.5–0.667), Q3 (1.5–2.0), and Q4 (>2.0), we utilized KEGG pathway enrichment analysis to discern pathway variances among these quartiles (Fig. 7*B*). Our findings indicate an obviously downregulation of focal adhesion, actin cytoskeleton regulation,

TABLE 6
Regulated Khib sites of plasma membrane

Gene name	Position	Amino acid	Disease/Health ratio	Disease/Health *p* value	Regulated type
ITGA1	766	K	0.216611009	0.006947307	Down
ITGA3	471	K	0.24808182	0.006644534	Down
ITGA3	1038	K	0.280791198	0.012598197	Down
ITGA7	335	K	0.359186993	0.018368475	Down
PSAP	303	K	0.382702437	0.011264876	Down
CACNA2D1	842	K	0.395615443	0.019808257	Down
GHITM	73	K	0.396422085	0.020435917	Down
DAG1	611	K	0.405304767	0.001216107	Down
SYPL1	179	K	0.433401843	0.04392602	Down
SEC62	60	K	0.437807702	0.036619378	Down
SERPINF1	134	K	1.536312557	0.0485295	Up

TABLE 7
Regulated Khib sites of APOB

Gene name	Position	Amino acid	Disease/Health ratio	Disease/Health *p* value	Regulated type
APOB	4465	K	0.49607701	0.047500988	Down
APOB	273	K	0.500563662	0.005278671	Down
APOB	1324	K	0.615933113	0.032245386	Down
APOB	110	K	0.641336329	0.04961298	Down
APOB	1476	K	0.647572589	0.044958988	Down
APOB	2640	K	0.665264301	0.022429164	Down
APOB	2340	K	1.573919855	0.017036071	Up
APOB	2428	K	1.813649847	0.01761469	Up

APOB, apolipoprotein B.

and tight junction pathways, while the Q4 group exhibited substantial alterations in thyroid hormone synthesis, HIF-1 signaling, and fructose and mannose metabolism (Fig. 7*C*). Specifically, Khib expression was markedly suppressed in pathways such as vascular smooth muscle contraction (Table 8), PI3K-Akt signaling (Table 9), and platelet activation (Table 10) in MetS patients with restenosis. Consequently, we employed the STRING database to construct protein–protein interaction (PPI) networks for these pathways to investigate their interactions further.

In the PPI network, we identified 28 proteins involved in the PI3K-Akt signaling pathway, 17 proteins associated with vascular smooth muscle contraction, and 8 proteins related to platelet activation. Within the vascular smooth muscle contraction pathways, MYH family proteins 9(K1845), 10(K203), and 11(K1710) exhibited different Khib modifications at various sites. Their Khib-modified MS/MS are shown in Supplemental Fig. S2. In the platelet activation pathway, 16 protein sites were modified, although the corresponding protein levels did not change significantly. To our surprise, among the listed proteins, only the expression and modification of COL1A1 showed completely opposite differences. The protein level of COL1A1 was upregulated by 2.83-fold in the disease group, whereas the Khib modification at K759 was downregulated by 0.51-fold in the disease group. Additionally, COL1A1 was implicated in the PI3K-Akt signaling pathway, with the most notable differential expression observed at position K277.

DISCUSSION

MetS is a prevalent metabolic disorder recognized as a major risk factor for coronary artery disease, significantly contributing to the global burden of cardiovascular diseases. Angioplasty remains the primary intervention for vascular occlusion, but the high incidence of postprocedural restenosis adversely affects patient outcomes (47). This underscores the necessity for a deeper investigation into the mechanisms driving restenosis. PTMs offer a more immediate and dynamic response compared to protein transcription or translation regulation in vascular pathologies (48–50). Although Khib modification is crucial in various pathologies, their study in cardiovascular contexts is limited. Our investigation employed quantitative proteomics and Khib PTM omics to examine vascular tissues from healthy individuals and patients with in-stent-induced restenosis. We conducted a statistical analysis of key regulatory pathways, proteins, and their modifications. Notably, pathways such as vascular smooth muscle contraction, PI3K-Akt signaling, and platelet activation were significantly downregulated in restenotic vessels of MetS patients.

Our study reveals that a significant portion of Khib-modified proteins are localized in the cytoplasm (41.4%). Functional categorization and pathway enrichment analyses illustrated that the modification disparities are prominent not only in proteins pivotal to organic and lipid metabolism, such as HSPA9 K368 and PRDX2 K10, which have direct links to MetS, but also in pathways associated with ISR, including smooth muscle contraction and platelet activation (51, 52). Furthermore, PRDX2 has been shown to mitigate iron-induced mitochondrial oxidative damage and lipid peroxidation, which is advantageous in addressing diabetic cardiac microvascular dysfunction (53). Meanwhile, upon focusing on the PPI network of these pathways, we observed an upregulation in the protein expression level of collagen type I alpha 1 (COL1A1) chain, while the modification level was decreased. COL1A1, encoding the primary component of type I collagen, is essential for the extracellular matrix and is implicated in vascular diseases such as aortic fibrosis, Marfan's syndrome, and aortic dissection (54–56). Sarohi *et al*. reported the altered levels of COL1A1 PTMs during metal stent and drug-eluting stent-induced neointima formation (57). Moreover, COL1A1 polymorphisms can impact blood lipid levels, particularly triglycerides (58). Its expression also shows significant differences in dyslipidemic patients with obesity, suggesting that variations in protein levels and modifications may influence the occurrence of restenosis. Consequently, these proteins with altered Khib modification patterns are likely involved in disease pathogenesis, either directly or indirectly.

In this manuscript, we focused on proteomics and PTMomics to comprehensively understand the differences in protein

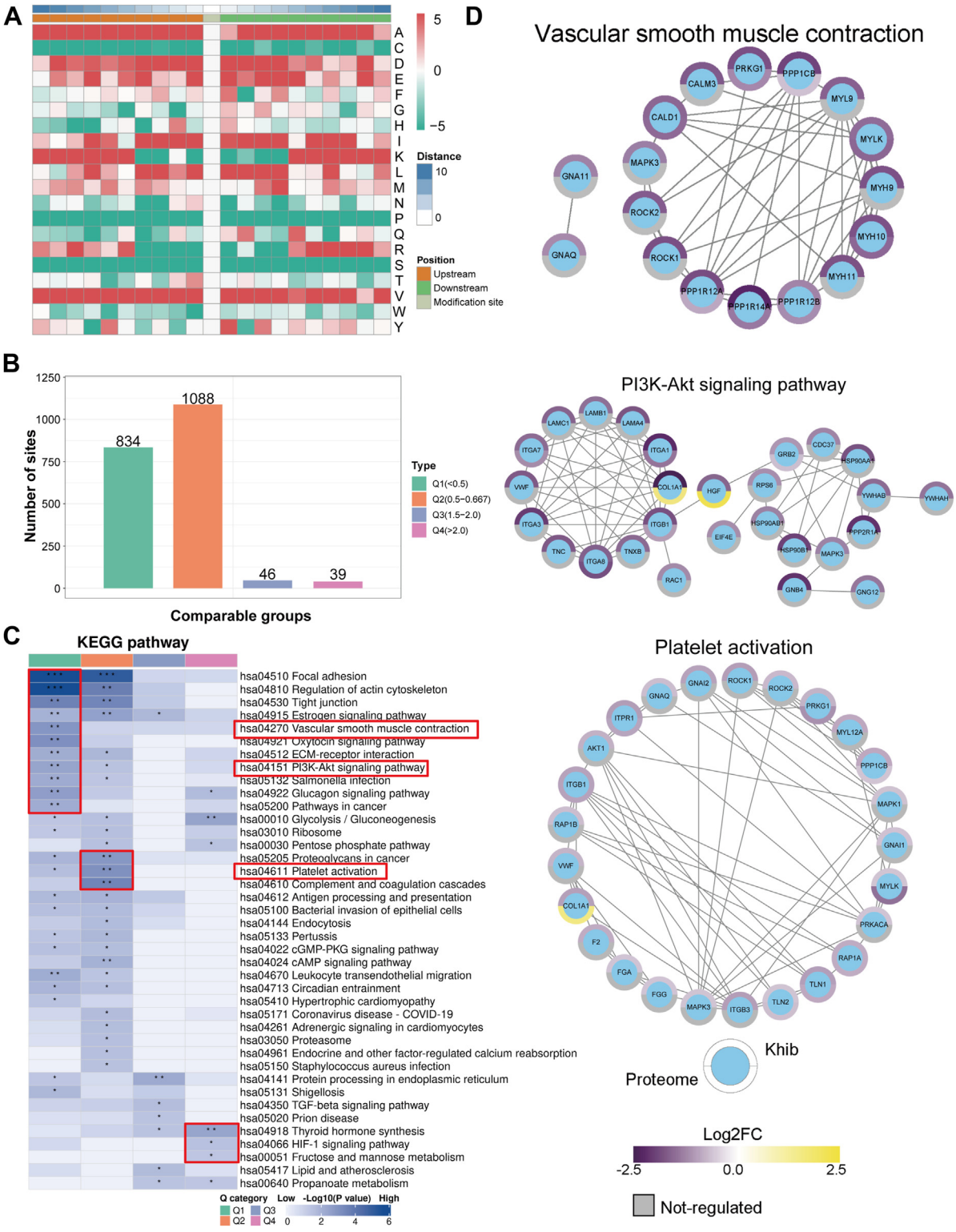

FIG. 7. **Characterization of metabolic syndrome-induced restenosis.** *A*, motif analysis of protein Khib sites, with *red* and *green* indicating upstream and downstream amino acid frequencies. *B* and *C*, the protein is divided into four parts according to the differential expression multiple, called Q1 to Q4 (Q1: <0.5, Q2: 0.5–1/1.5, Q3: 1.5–2.0, Q4: >2.0). *B*, quantity comparison bar chart for each group; *C*, KEGG pathway of the Khib proteome. *D*, vascular smooth muscle contraction, PPI network of PI3K-Akt signaling pathway and Platelet activation. The first two analyze Q1 and the third group Q2. The *upper part* represents Khib modification (the modification site with the largest difference in the protein), the *lower part* represents the proteome, *purple* indicates downregulated protein, *yellow* indicates upregulated protein, the darker the color, the larger the difference multiple, and *gray* represents no significant difference. KEGG, Kyoto Encyclopedia of Genes and Genomes.

TABLE 8
Downregulated Khib sites of vascular smooth muscle contraction

Gene name	Position	Amino acid	Disease/Health ratio	Disease/Health *p* value	Regulated type
PPP1R14A	54	K	0.227818019	0.004006594	Down
PPP1CB	303	K	0.285787383	0.011572711	Down
PPP1R12A	320	K	0.306656151	0.015547544	Down
ROCK1	310	K	0.310265111	0.006767067	Down
PRKG1	410	K	0.310362739	0.020466805	Down
MYH11	1710	K	0.314571369	0.018091255	Down
MYH9	1845	K	0.316347343	0.007689433	Down
MYH10	203	K	0.316870096	0.006735028	Down
CALM3	78	K	0.329408266	0.005815807	Down
ROCK2	995	K	0.337417719	0.031967095	Down
MYL9	51	K	0.351658333	0.011420605	Down
CALD1	380	K	0.36403842	0.046478537	Down
MYLK	1202	K	0.3799004	0.001557424	Down
MAPK3	302	K	0.427910164	0.00344306	Down
GNA11	120	K	0.436568229	0.021677017	Down
PPP1R12B	895	K	0.445464265	0.023520083	Down
GNAQ	72	K	0.462235068	0.001025703	Down

levels and modification sites involved in MetS-induced restenosis. Nevertheless, the accuracy of these findings requires further validation through both *in vivo* and *in vitro* models. Based on the IHC results of animal restenosis tissues, we preliminarily analyzed that the intimal expression differed significantly, and the modification was markedly reduced in the disease group, suggesting that Khib may play a protective role in MetS-induced restenosis. The next step is to select key modification sites for knockout in *in vivo* and *in vitro* models and to assess vascular function to further elucidate the role of Khib modification in the occurrence and progression of the disease.

TABLE 9
Downregulated Khib sites of PI3K-Akt signaling pathway

Gene name	Position	Amino acid	Disease/Health ratio	Disease/Health *p* value	Regulated type
COL1A1	277	K	0.183529137	0.001782291	Down
ITGA1	766	K	0.216611009	0.006947307	Down
PPP2R1A	272	K	0.228838591	0.000807033	Down
GNB4	209	K	0.229543618	0.004950945	Down
ITGA3	471	K	0.24808182	0.006644534	Down
HSP90B1	486	K	0.261859658	0.006836258	Down
ITGB1	73	K	0.294390946	0.011368364	Down
HSP90AA1	292	K	0.296118277	0.023633689	Down
LAMA4	425	K	0.299848203	0.001745851	Down
VWF	1423	K	0.309445426	0.024061825	Down
TNC	942	K	0.3104142	0.006275539	Down
ITGA8	141	K	0.329162286	0.030421152	Down
LAMC1	164	K	0.334450955	0.001150648	Down
HGF	91	K	0.341558837	0.000026171	Down
PRKAA1	280	K	0.347703947	0.037903363	Down
TNXB	3524	K	0.356382584	0.003020057	Down
ITGA7	335	K	0.359186993	0.018368475	Down
YWHAB	29	K	0.360460353	0.040999849	Down
LAMB1	1688	K	0.371296893	0.049266809	Down
YWHAH	110	K	0.386026192	0.025498852	Down
GNG12	4	K	0.39318199	0.002198722	Down
HSP90AB1	435	K	0.419850928	0.032577683	Down
MAPK3	302	K	0.427910164	0.00344306	Down
CDC37	276	K	0.437625535	0.031594806	Down
RAC1	147	K	0.448775825	0.026726445	Down
EIF4E	162	K	0.465346296	0.004360292	Down
RPS6	58	K	0.467913893	0.020760974	Down

TABLE 10
Downregulated Khib sites of platelet activation

Gene name	Position	Amino acid	Disease/Health ratio	Disease/Health *p* value	Regulated type
ITPR1	249	K	0.500396834	0.001850384	Down
ITGB3	443	K	0.503911529	0.006730388	Down
ROCK1	1208	K	0.50521864	0.03396109	Down
TLN1	1190	K	0.507745687	0.002290137	Down
COL1A1	759	K	0.512683646	0.031230116	Down
ITGB1	349	K	0.518992016	0.002808446	Down
GNAI2	54	K	0.519301743	0.031846138	Down
PPP1CB	25	K	0.548159112	0.035934653	Down
MYL12A	150	K	0.548399168	0.014564421	Down
RAP1A	117	K	0.558600196	0.003247042	Down
F2	344	K	0.561272815	0.019170586	Down
AKT1	284	K	0.574883054	0.006681717	Down
PRKG1	499	K	0.585063417	0.004620814	Down
VWF	1430	K	0.589850555	0.042125824	Down
ROCK2	511	K	0.612070059	0.02236173	Down
RAP1B	117	K	0.628966657	0.018538609	Down
GNAQ	107	K	0.629018064	0.007930137	Down
MAPK1	138	K	0.644478699	0.016115143	Down
GNAI1	67	K	0.650729021	0.034786832	Down
MYLK	1721	K	0.653142708	0.013865328	Down
MAPK3	361	K	0.655676767	0.049352369	Down
FGG	188	K	0.658975449	0.01687466	Down
FGA	243	K	0.658975449	0.01245972	Down
PRKACA	30	K	0.660362436	0.013950963	Down
TLN2	348	K	0.662256683	0.047347989	Down

In summary, our study is the first to investigate the differential expression of proteins and Khib modifications in MetS-induced restenosis. Despite its innovative nature, the study has its limitations: it identifies significantly altered proteins and modification sites but does not elucidate precise regulatory mechanisms or identify downstream effectors. These findings will guide further research into the effects of PTMs in vascular diseases caused by metabolic disorders and establish a foundation for future targeted therapeutic strategies for ISR.

DATA AVAILABILITY

The raw LC-MS/MS files and peptide/protein/modification identification have been deposited to the ProteomeXchange Consortium via the PRIDE partner repository with the dataset identifier PXD062384. Annotated spectra for identified proteomics and Khib modifications have been deposited on MS-viewer with the search key "4xxtqp3gqg" and "kc21vnele4".

Supporting information—This article contains supporting information.

Author Contributions—X. L., L. Z., W. H., and Yijin. Y. data curation; X. L. and L. Z. software; X. L. and W. H. validation; X. L., writing–original draft; Y. Y., T. Y., and Y. L. writing–review and editing; Y. Y. and M. G. resources; Yijun. Y. and M. G. methodology; Yijun. Y. and T. L. visualization; T. L. investigation; T. Y. conceptualization.

Funding and Additional Information—This work was supported by the National Natural Science Foundation of China (No. 82270518, 82270442), Taishan Scholar Program of Shandong Province (No. tsqn202408156), Qingdao West Coast New Area Science and Technology Project (No. 2022–57), and the Natural Science Foundation of Shandong Province (No. ZR2022MH031).

Conflict of Interest—The authors declare no competing interests.

Abbreviations—The abbreviations used are: COL1A1, collagen type I alpha 1; DEPs, differentially expressed proteins; ER, endoplasmic reticulum; GO, Gene Ontology; IHC, immunohistochemistry; ISR, in-stent restenosis; KEGG, Kyoto Encyclopedia of Genes and Genomes; MetS, metabolic syndrome; PPI, protein–protein interaction; PTM, post-translational modification.

Received October 29, 2024, and in revised form, April 21, 2025
Published, MCPRO Papers in Press, April 24, 2025, https://doi.org/10.1016/j.mcpro.2025.100978

REFERENCES

1. Criqui, M. H., Matsushita, K., Aboyans, V., Hess, C. N., Hicks, C. W., Kwan, T. W., *et al*. (2021) Lower extremity peripheral artery disease: contemporary epidemiology, management gaps, and future directions: a scientific statement from the American heart association. *Circulation* **144**, e171–e191

2. Criqui, M. H., and Aboyans, V. (2015) Epidemiology of peripheral artery disease. *Circ. Res.* **116**, 1509–1526
3. Pabon, M., Cheng, S., Altin, S. E., Sethi, S. S., Nelson, M. D., Moreau, K. L., *et al*. (2022) Sex differences in peripheral artery disease. *Circ. Res.* **130**, 496–511
4. Beckman, J. A., Schneider, P. A., and Conte, M. S. (2021) Advances in revascularization for peripheral artery disease: revascularization in PAD. *Circ. Res.* **128**, 1885–1912
5. Ho, K. J., and Owens, C. D. (2017) Diagnosis, classification, and treatment of femoropopliteal artery in-stent restenosis. *J. Vasc. Surg.* **65**, 545–557
6. Hiramoto, J. S., Teraa, M., de Borst, G. J., and Conte, M. S. (2018) Interventions for lower extremity peripheral artery disease. *Nat. Rev. Cardiol.* **15**, 332–350
7. Kastrati, A., Mehilli, J., Dirschinger, J., Pache, J., Ulm, K., Schühlen, H., *et al*. (2001) Restenosis after coronary placement of various stent types. *Am. J. Cardiol.* **87**, 34–39
8. Thukkani, A. K., and Kinlay, S. (2015) Endovascular intervention for peripheral artery disease. *Circ. Res.* **116**, 1599–1613
9. Jakubiak, G. K., Pawlas, N., Cieślar, G., and Stanek, A. (2021) Pathogenesis and clinical significance of in-stent restenosis in patients with diabetes. *Int. J. Environ. Res. Public Health* **18**, 11970
10. Tocci, G., Barbato, E., Coluccia, R., Modestino, A., Pagliaro, B., Mastromarino, V., *et al*. (2016) Blood pressure levels at the time of percutaneous coronary revascularization and risk of coronary in-stent restenosis. *Am. J. Hypertens.* **29**, 509–518
11. Topakian, R., Sonnberger, M., Nussbaumer, K., Haring, H. P., Trenkler, J., and Aichner, F. T. (2008) Postprocedural high-density lipoprotein cholesterol predicts carotid stent patency at 1 year. *Eur. J. Neurol.* **15**, 179–184
12. Wu, B. J., Li, Y., Ong, K. L., Sun, Y., Shrestha, S., Hou, L., *et al*. (2017) Reduction of in-stent restenosis by cholesteryl ester transfer protein inhibition. *Arteriosclerosis, Thromb. Vasc. Biol.* **37**, 2333–2341
13. Qin, Z., Zhou, K., Li, Y. P., Wang, J. L., Cheng, W. J., Hu, C. P., *et al*. (2019) Remnant lipoproteins play an important role of in-stent restenosis in type 2 diabetes undergoing percutaneous coronary intervention: a single-centre observational cohort study. *Cardiovasc. diabetology* **18**, 1–9
14. Qin, Z., Zheng, F. W., Zeng, C., Zhou, K., Geng, Y., Wang, J. L., *et al*. (2017) Elevated levels of very low-density lipoprotein cholesterol independently associated with in-stent restenosis in diabetic patients after drug-eluting stent implantation. *Chin. Med. J.* **130**, 2326–2332
15. Piatti, P., Di Mario, C., Monti, L. D., Fragasso, G., Sgura, F., Caumo, A., *et al*. (2003) Association of insulin resistance, hyperleptinemia, and impaired nitric oxide release with in-stent restenosis in patients undergoing coronary stenting. *Circulation* **108**, 2074–2081
16. Santos-Pardo, I., Andersson Franko, M., Lagerqvist, B., Ritsinger, V., Eliasson, B., Witt, N., *et al*. (2024) Glycemic control and coronary stent failure in patients with type 2 diabetes mellitus. *J. Am. Coll. Cardiol.* **84**, 260–272
17. Bai, X. S., Feng, Y., Wang, T., Zhang, X., Yang, C. L., Wang, Y. B., *et al*. (2020) Impact of metabolic syndrome on short-term outcome of carotid revascularization: a large sample size study in Chinese population. *Chin Med. J. (Engl)* **133**, 2688–2695
18. Sasso, F. C., Pafundi, P. C., Marfella, R., Calabrò, P., Piscione, F., Furbatto, F., *et al*. (2019) Adiponectin and insulin resistance are related to restenosis and overall new PCI in subjects with normal glucose tolerance: the prospective AIRE Study. *Cardiovasc. Diabetol.* **18**, 24
19. Chen, L., Liu, S., and Tao, Y. (2020) Regulating tumor suppressor genes: post-translational modifications. *Signal. Transduct Target Ther.* **5**, 90
20. Zhu, S., Zhu, W., Zhao, K., Yu, J., Lu, W., Zhou, R., *et al*. (2024) Discovery of a novel hybrid coumarin-hydroxamate conjugate targeting the HDAC1-Sp1-FOSL2 signaling axis for breast cancer therapy. *Cell Commun. Signal.* **22**, 361
21. Wang, C., Yu, B., Zhou, H., Li, H., Li, S., Li, X., *et al*. (2025) tRF-AspGTC promotes intracranial aneurysm formation by controlling TRIM29-mediated galectin-3 ubiquitination. *Research (Wash D C)* **8**, 0574
22. Gao, J., Shao, K., Chen, X., Li, Z., Liu, Z., Yu, Z., *et al*. (2020) The involvement of post-translational modifications in cardiovascular pathologies: focus on SUMOylation, neddylation, succinylation, and prenylation. *J. Mol. Cell Cardiol* **138**, 49–58
23. Li, X., Yang, Y., Zhang, B., Lin, X., Fu, X., An, Y., *et al*. (2022) Lactate metabolism in human health and disease. *Signal. Transduct Target Ther.* **7**, 305
24. Li, M., Li, G., Yang, Y., Zong, J., Fu, X., Htet, A. L. H., *et al*. (2023) piRNA-823 is a novel potential therapeutic target in aortic dissection. *Pharmacol. Res.* **196**, 106932
25. Li, M., Li, S., and Zhang, L. (2023) Phosphorylation promotes the accumulation of PERIOD protein foci. *Research (Wash D C)* **6**, 0139
26. Du, Y., Zhu, P., Li, Y., Yu, J., Xia, T., Chang, X., *et al*. (2024) DNA-PKcs phosphorylates Cofilin2 to induce endothelial dysfunction and microcirculatory disorder in endotoxemic cardiomyopathy. *Research (Wash D C)* **7**, 0331
27. Dai, L., Peng, C., Montellier, E., Lu, Z., Chen, Y., Ishii, H., *et al*. (2014) Lysine 2-hydroxyisobutyrylation is a widely distributed active histone mark. *Nat. Chem. Biol.* **10**, 365–370
28. Huang, H., Tang, S., Ji, M., Tang, Z., Shimada, M., Liu, X., *et al*. (2018) p300-Mediated lysine 2-hydroxyisobutyrylation regulates glycolysis. *Mol. Cell* **70**, 663–678.e6
29. Ge, H., Li, B., Chen, W., Xu, Q., Chen, S., Zhang, H., *et al*. (2019) Differential occurrence of lysine 2-hydroxyisobutyrylation in psoriasis skin lesions. *J. Proteomics* **205**, 103420
30. Liao, L., He, Y., Li, S. J., Yu, X. M., Liu, Z. C., Liang, Y. Y., *et al*. (2023) Lysine 2-hydroxyisobutyrylation of NAT10 promotes cancer metastasis in an ac4C-dependent manner. *Cell Res.* **33**, 355–371
31. Zhang, Z., Wang, Y., Liang, Z., Meng, Z., Zhang, X., Ma, G., *et al*. (2023) Modification of lysine-260 2-hydroxyisobutyrylation destabilizes ALDH1A1 expression to regulate bladder cancer progression. *iScience* **26**, 108142
32. Cheng, Y. M., Peng, Z., Chen, H. Y., Pan, T. T., Hu, X. N., Wang, F., *et al*. (2020) Posttranslational lysine 2-hydroxyisobutyrylation of human sperm tail proteins affects motility. *Hum. Reprod.* **35**, 494–503
33. Li, X., Yu, T., Li, X., He, X., Zhang, B., and Yang, Y. (2024) Role of novel protein acylation modifications in immunity and its related diseases. *Immunology* **173**, 53–75
34. Huang, H., Luo, Z., Qi, S., Huang, J., Xu, P., Wang, X., *et al*. (2018) Landscape of the regulatory elements for lysine 2-hydroxyisobutyrylation pathway. *Cell Res* **28**, 111–125
35. Wilson, P. W., D'Agostino, R. B., Parise, H., Sullivan, L., and Meigs, J. B. (2005) Metabolic syndrome as a precursor of cardiovascular disease and type 2 diabetes mellitus. *Circulation* **112**, 3066–3072
36. Liu, Y., Yang, Y., Li, M., Fu, X., He, X., Li, X., *et al*. (2024) CircTMEM165 facilitates endothelial repair by modulating mitochondrial fission via miR-192/SCP2 in vitro and in vivo. *iScience* **27**, 109502
37. Li, X., Yang, Y., Wang, Z., Lin, X., Fu, X., He, X., *et al*. (2024) CircHIPK3 targets DRP1 to mediate hydrogen peroxide-induced necroptosis of vascular smooth muscle cells and atherosclerotic vulnerable plaque formation. *J. Adv. Res.* **69**, 329–341
38. Perez-Riverol, Y., Bai, J., Bandla, C., García-Seisdedos, D., Hewapathirana, S., Kamatchinathan, S., *et al*. (2022) The PRIDE database resources in 2022: a hub for mass spectrometry-based proteomics evidences. *Nucleic Acids Res.* **50**, D543–D552
39. Douglas, G., Van Kampen, E., Hale, A. B., McNeill, E., Patel, J., Crabtree, M. J., *et al*. (2013) Endothelial cell repopulation after stenting determines in-stent neointima formation: effects of bare-metal vs. drug-eluting stents and genetic endothelial cell modification. *Eur. Heart J.* **34**, 3378–3388
40. Kipshidze, N., Dangas, G., Tsapenko, M., Moses, J., Leon, M. B., Kutryk, M., and Serruys, P. (2004) Role of the endothelium in modulating neointimal formation: vasculoprotective approaches to attenuate restenosis after percutaneous coronary interventions. *J. Am. Coll. Cardiol.* **44**, 733–739
41. Alfonso, F., Byrne, R. A., Rivero, F., and Kastrati, A. (2014) Current treatment of in-stent restenosis. *J. Am. Coll. Cardiol.* **63**, 2659–2673
42. Niemann, M., Wiese, S., Mani, J., Chanfon, A., Jackson, C., Meisinger, C., *et al*. (2013) Mitochondrial outer membrane proteome of Trypanosoma brucei reveals novel factors required to maintain mitochondrial morphology. *Mol. Cell Proteomics* **12**, 515–528
43. Meier, F., Brunner, A. D., Koch, S., Koch, H., Lubeck, M., Krause, M., *et al*. (2018) Online Parallel accumulation-serial fragmentation (PASEF) with a novel trapped ion mobility mass spectrometer. *Mol. Cell Proteomics* **17**, 2534–2545

44. Montasser, M. E., O'Hare, E. A., Wang, X., Howard, A. D., McFarland, R., Perry, J. A., *et al*. (2018) An APOO pseudogene on chromosome 5q is associated with low-density lipoprotein cholesterol levels. *Circulation* **138**, 1343–1355
45. Gallo, S., Sala, V., Gatti, S., and Crepaldi, T. (2015) Cellular and molecular mechanisms of HGF/Met in the cardiovascular system. *Clin. Sci.* **129**, 1173–1193
46. Gary, T., Rief, P., Stojakovic, T., Froehlich, H., Scharnagl, H., Hafner, F., *et al*. (2011) Lipoproteins and the development of restenosis after stent implantation in the superficial femoral artery in patients with peripheral artery disease. *Cardiovasc. Interv. Radiol.* **34**, 739–743
47. Deedwania, P. C. (2004) Metabolic syndrome and vascular disease: is nature or nurture leading the new epidemic of cardiovascular disease? *Circulation* **109**, 2–4
48. Xue, Q., Yang, Y., Li, H., Li, X., Zou, L., Li, T., *et al*. (2023) Functions and mechanisms of protein lysine butyrylation (Kbu): therapeutic implications in human diseases. *Genes Dis.* **10**, 2479–2490
49. Zou, L., Yang, Y., Wang, Z., Fu, X., He, X., Song, J., *et al*. (2023) Lysine malonylation and its links to metabolism and diseases. *Aging Dis.* **14**, 84–98
50. Jiang, X., Yang, Y., Li, X., Li, T., Yu, T., and Fu, X. (2024) Lactylation: an innovative approach to disease control. *Aging Dis.* https://doi.org/10.14336/AD.2024.0918
51. Zhang, X., Chen, X., Qi, T., Kong, Q., Cheng, H., Cao, X., *et al*. (2019) HSPA12A is required for adipocyte differentiation and diet-induced obesity through a positive feedback regulation with PPARgamma. *Cell Death Differ* **26**, 2253–2267
52. Kim, Y. N., Shin, J. H., Kyeong, D. S., Cho, S. Y., Kim, M. Y., Lim, H. J., *et al*. (2021) Ahnak deficiency attenuates high-fat diet-induced fatty liver in mice through FGF21 induction. *Exp. Mol. Med.* **53**, 468–482
53. Chen, Y., Li, S., Yin, M., Li, Y., Chen, C., Zhang, J., *et al*. (2023) Isorhapontigenin attenuates cardiac microvascular injury in diabetes via the inhibition of mitochondria-associated ferroptosis through PRDX2-MFN2-ACSL4 pathways. *Diabetes* **72**, 389–404
54. Rahkonen, O., Su, M., Hakovirta, H., Koskivirta, I., Hormuzdi, S. G., Vuorio, E., *et al*. (2004) Mice with a deletion in the first intron of the Col1a1 gene develop age-dependent aortic dissection and rupture. *Circ. Res.* **94**, 83–90
55. Lim, W. W., Dong, J., Ng, B., Widjaja, A. A., Xie, C., Su, L., *et al*. (2022) Inhibition of IL11 signaling reduces aortic pathology in murine marfan syndrome. *Circ. Res.* **130**, 728–740
56. Raaz, U., Schellinger, I. N., Chernogubova, E., Warnecke, C., Kayama, Y., Penov, K., *et al*. (2015) Transcription factor Runx2 promotes aortic fibrosis and stiffness in type 2 diabetes mellitus. *Circ. Res.* **117**, 513–524
57. Sarohi, V., and Basak, T. (2023) Perturbed post-translational modification (PTM) network atlas of collagen I during stent-induced neointima formation. *J. Proteomics* **276**, 104842
58. Miao, L., Yin, R. X., Pan, S. L., Yang, S., Yang, D. Z., and Lin, W. X. (2019) Circulating miR-3659 may be a potential biomarker of dyslipidemia in patients with obesity. *J. Transl. Med.* **17**, 25